Anahid Khoobyar
Department of Aerospace and Mechanical Engineering,
University of Southern California,
USC Viterbi School of Engineering,
Los Angeles, CA 90089-1453

Anita N. Penkova
Assistant Professor
Department of Aerospace and Mechanical Engineering,
USC Viterbi School of Engineering,
Los Angeles, CA 90089-1453;
Saban Research Institute,
Children's Hospital Los Angeles,
Los Angeles, CA 90027

Mark S. Humayun
Cornelius Pings Professor of Biomedical Sciences,
Professor of Ophthalmology, Biomedical Engineering, and Integrative Anatomical Sciences,
Director, USC Ginsburg Institute for Biomedical Therapeutics,
Co-Director USC Roski Eye Institute,
Department of Ophthalmology,
Keck School of Medicine,
University of Southern California,
Los Angeles, CA 90033-4682

Satwindar Singh Sadhal[1]
Professor
Department of Aerospace and Mechanical Engineering,
University of Southern California,
USC Viterbi School of Engineering,
Los Angeles, CA 90089-1453;
Children's Hospital Los Angeles,
Saban Research Institute,
Los Angeles, CA 90027;
Department of Ophthalmology,
Keck School of Medicine,
University of Southern California,
Los Angeles, CA 90033-4682
e-mail: sadhal@usc.edu

Mathematical Model of Macromolecular Drug Transport in a Partially Liquefied Vitreous Humor

The purpose of this study is to investigate the effect of partial liquefaction (due to ageing) of the vitreous humor on the transport of ocular drugs. In our model, the gel part of the vitreous is treated as a Darcy-type porous medium. A spherical region within the porous part of vitreous is in a liquid state which, for computational purposes, is also treated as a porous medium but with a much higher permeability. Using the finite element method, a time-dependent, three-dimensional model has been developed to computationally simulate (using the Petrov–Galerkin method) the transport of intravitreally injected macromolecules where both convection and diffusion are present. From a fluid physics and transport phenomena perspective, the results show many interesting features. For pressure-driven flow across the vitreous, the flow streamlines converge into the liquefied region as the flow seeks the fastest path of travel. Furthermore, as expected, with increased level of liquefaction, the overall flow rate increases for a given pressure drop. We have quantified this effect for various geometrical considerations. The flow convergence into the liquefied region has important implication for convective transport. One effect is the clear diversion of the drug as it reaches the liquefied region. In some instances, the entry point of the drug in the retinal region gets slightly shifted due to liquefaction. While the model has many approximations and assumptions, the focus is illustrating the effect of liquefaction as one of the building blocks toward a fully comprehensive model. [DOI: 10.1115/1.4053197]

Keywords: ocular drug delivery, vitreous liquefaction, mass transfer

1 Introduction

Syneresis, or partial liquefaction of the vitreous humor, is most common among the elderly and is associated with retinal detachment, macular holes, and vitreoretinal degeneration. For the purpose of targeted drug delivery, it is beneficial and clinically important to understand how the degree of vitreous liquefaction influences drug kinetics and transport. Such effort will contribute to the development of predictive numerical models for intravitreal drug transport leading to improved individualized treatment of patients with ocular diseases.

Current treatments for posterior eye pathologies such as age-related macular degeneration and diabetic retinopathy include intravitreal delivery of small molecules and macromolecular drugs that have proven to be among the most effective pathway compared to other ocular drug delivery mechanisms [1]. In the U.S. alone, a million patients are being treated by administering the drug intravitreally (injection, implant) [2–4]. While intravitreal treatment is the most frequently used procedure, it is not completely understood how the drug intervention works in the heterogeneous vitreous medium in terms of transport. Drug distribution in the vitreous humor depends on the individual human anatomy, shape of the eye, and vitreous properties such as the degree of syneresis and ocular topography. Hence, our long-term goal here is to establish a detailed, comprehensive time-dependent, three-dimensional model for the intravitreal drug delivery that would greatly improve the efficacy and recommend safety levels of this therapeutic treatment. Such a model entails several types of physiological phenomena that need to be implemented. The current scope is however limited to analyzing the effect of liquefaction and the role it plays in drug distribution. Intravitreal drug transport has been analyzed theoretically and experimentally in several works [5–11]. In the last thirty years, modeling and computer

[1]Corresponding author.

Contributed by the Heat Transfer Division of ASME for publication in the Journal of Heat Transfer. Manuscript received September 4, 2021; final manuscript received December 1, 2021; published online February 7, 2022. Assoc. Editor: Ram Devireddy.

simulation of ocular drug distribution began with various researchers including Araiel et al. [12], followed by Tojo et al. [13] and Friedrich et al. [14]. Some of the investigators assumed the vitreous humor as a homogeneous medium (all gel or all liquid). With all-liquid systems, the vitreous humor has been modeled as a viscous Newtonian fluid while all-gel systems have applied Darcy flow. Tojo and Isowaki [7] presented an intravitreal drug transport analysis using a cylindrical model of the eye based on Fick's law of diffusion and neglected the convective transport. However, metabolic consumption rate was considered in this model. In later attempts to model intravitreal drug transport, convection driven by a pressure drop between the hyaloid membrane and retina has been taken into consideration, but still the boundary conditions imposed in the models and physical structure and topography of the vitreous are oversimplified. Friedrich et al. [14] used the finite element method to analyze mass-transfer problem in a homogeneous vitreous using simplified cylindrical vitreous body model. They accurately describe the geometry of the eye, and both diffusive and convective mass transfers were taken into account. However, as already mentioned, the vitreous humor was modeled as a homogeneous medium. Lin et al. [15] improved the simulation model developed by Firedrich [14] in terms of more appropriate boundary conditions and geometry of the injected drug. Xu et al. [16] explored a two-dimensional model including diffusion and convection effects on drug released from a cylindrical source in the vitreous. Xu et al. [17] developed a three-dimensional strategy for the prediction of drug distribution following intravitreally injected polymer microspheres from a point source. A three-dimensional finite element model has been suggested by Park et al. [18] to simulate transport processes in rabbit eye from both intravitreal injection and controlled release implant for an application in the treatment of retinal disease. All mentioned studies, with some exceptions, assumed that the working fluid is the vitreous and treated it as a porous medium. Drug transport has been modeled as a diffusive transport together with convection by Darcy flow.

2 Assumptions and Approximations

As mentioned earlier, the fully comprehensive transport model for the eye is quite complicated and encompasses many physiological phenomena that need to be implemented. Our goal in this work is to isolate the effect of syneresis from the perspective of pressure-driven transport of water in the system. With this limited scope, we mention below the various other effects that may influence drug transport but are not included in the paper.

2.1 Saccadic Motion. Without any liquefaction, the eye motion causes little in the way of fluid transport in the vitreous. However, with the presence of liquid pockets, the oscillatory motion of the eyes can create circulatory currents [19,20]. Rotational oscillatory motions can lead to streaming, which, compared to pressure-driven transport, can be significant within the liquid portion [19].

2.2 Vitreous Structural Flexibility. The vitreous is a viscoelastic structure that with liquefaction can experience distortion due to saccadic motion [20]. This again is a complex piece of the comprehensive model that will be implemented as the model developed further. For the current model, the vitreous is approximated to be a rigid structure.

2.3 Hindrance Effect. Macromolecules can experience hindrance when moving through a fine porous structure. This can be effectively modeled with modified fluid velocity in the advection term. However, currently our experimental research on measuring the hindrance coefficient is undergoing and data in yet unavailable. Besides, the hindrance effect does not take away the basic structure of drug transport other than reducing the advection.

2.4 Thermal Effects. The role of naturally occurring thermal effects is expected to be minimal in terms of intravitreal drug transport. Very recent studies by Huang and Gharib [21] have shown experimentally that an imposed thermal stimulus on a fully liquid vitreous (experimental simulation model), buoyant convection can be significant. Also, Narasimhan and Sundarraj [22] investigated the thermal effects in a fully liquid vitreous. Naturally occurring thermal gradients in the liquefied region may have a small contribution, and this again will be a part of a comprehensive model presently under development.

3 Mathematical Modeling

Fluid mechanics and drug transport within the vitreous humor can be adequately described by established equations of momentum and mass conservation. Typically, fluid flow requires solution to the Navier–Stokes equations while mass transfer involves the convection-diffusion equation. The review by Mukundakrishnan [23] adequately describes modeling of solute transport in living tissue. We make appropriate approximations relevant to transport in the vitreous humor. These are discussed in Sec. 3.1.

We are considering a human eye in which water transport takes place from the anterior chamber (aqueous humor) through the vitreous humor and retinal pigment epithelium (RPE) and into the bloodstream [24], as shown in Fig. 1. The drug is dispensed by injection into the vitreous humor where the physiological flow of water described above convects it toward the retina. At the same time, Fick's law-type diffusion takes place within the vitreous. To solve this set of equations, an in-house computational model using MATLAB was developed to quantify and illustrate the drug transport in the heterogeneous vitreous. Details of the computational procedure are given in the Supplemental Material on the ASME Digital Collection.

A finite element method was implemented to model the convective and diffusive transport of intravitreally delivered macromolecules over time. The geometry of the model was created with Solidworks as shown in Fig. 2.

3.1 Fluid Mechanics: Pressure and Velocity Distributions. The vitreous is a gel-like material that consists of mostly water in a fibrous meshwork of collagen and hyaluronic acid [25,26]. This composition gives the vitreous a porous medium characterization. Therefore, fluid transport in the vitreous can be described very well by the Darcy flow approximation of the Navier–Stokes equations [17]. The liquefied region is assumed to be a porous medium as well but with a thousand times higher permeability than the nonliquefied zone. Thus, for practical purposes, the highly porous spherical region is essentially a liquid. This procedure is effective in overcoming the difficulties that one encounters with the treatment of fluid flow in multiregion systems with different

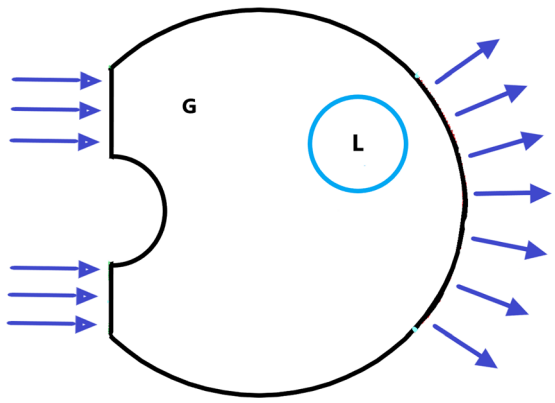

Fig. 1 Underlying sketch for the eye model, L: liquefied region, G: nonliquefied (gel) region

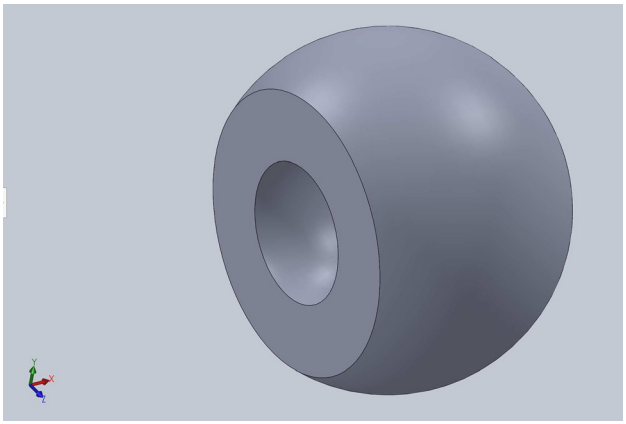

Fig. 2 A model of the eye created with SOLIDWORKS

characterization of Navier–Stokes equation. Nevertheless, it is understood that with this Darcy-flow model, the tangential velocity and shear stress conditions at the gel–liquid interface need to be relaxed. The core principle in allowing this model is the extremely low permeability of the gel part of the vitreous while the liquid part experiences little resistance in comparison. Undoubtedly, this aspect needs deeper examination and we are presently investigating further. As mentioned earlier, the purpose of this work is to illustrate approximately the effect of partial liquefaction on the fluid flow characterization related to mass transfer.

Pressure and velocity in this medium follow Darcy and continuity equations [27–30]:

$$\boldsymbol{u}_{\mathrm{L}} = -\frac{K_{\mathrm{L}}}{\mu}\nabla P_{\mathrm{L}} \tag{1}$$

$$\boldsymbol{u}_{\mathrm{G}} = -\frac{K_{\mathrm{G}}}{\mu}\nabla P_{\mathrm{G}} \tag{2}$$

where K values refer to the corresponding Darcy coefficients of the gel and the liquid parts of the vitreous, and μ refers to the dynamic viscosity of the liquefied region as well as the liquid part of the gel meshwork. The subscripts G and L refer to the gel and liquid regions, respectively, within the vitreous. Measurement of the hydraulic conductivity has been carried out by Penkova et al. [25] and Xu et al. [16]. We have used the value in the work done by Penkova [25]

$$\frac{K_{\mathrm{G}}}{\mu} = 9\times 10^{-6}\,\frac{\mathrm{mm}^2}{\mathrm{Pa}\cdot\mathrm{s}}, \quad \frac{K_{\mathrm{L}}}{K_{\mathrm{G}}} = 10^3$$

This value is approximate and a measurement for the human vitreous does not seem to be available. Furthermore, there is likely to be variation between different individuals. After applying continuity equation ($\nabla\cdot\boldsymbol{u}_{\mathrm{i}} = 0$, $\mathrm{i} = \mathrm{L}, \mathrm{G}$) to Eqs. (1) and (2), we obtain

$$\nabla^2 P_{\mathrm{L}} = 0, \quad \nabla^2 P_{\mathrm{G}} = 0 \tag{3}$$

As mentioned earlier, the direction of the water flow is taken to be from anterior chamber to posterior sector of the eye. The inlet and outlet of water flow are displayed in Fig. 1.

We assume that the fluid from aqueous humor enters the vitreous through the hyaloid membrane and exits through the retina into the bloodstream. The following boundary condition is considered for inlet and outlet:

$$\boldsymbol{u}_{\mathrm{in}} = 0.000147 \simeq 0.00015\,\mathrm{mm/s} \qquad P_{\mathrm{out}} = 0\,\mathrm{Pa} \tag{4}$$

The remainder of the vitreous in contact with the wall of the eye and the lens is assumed to have no penetration, and thus zero normal velocity ($\boldsymbol{u}\cdot\boldsymbol{n} = 0$). Again, there is some degree of flow into the choroid through the inner sidewalls (see, e.g., Ref. [16]). Since our focus is on the effect of syneresis on the bulk of the flow, we approximate the flow outside the retinal region as negligible. The velocity of the inlet domain was calculated by taking the volumetric flow rate of the water from the inlet ($3\,\mu\mathrm{l/min}$ [31]) divided by the inlet area ($3.4\,\mathrm{cm}^2$). It is understood that for a given geometry, only the difference in the pressure determines the flow rate. Therefore, we have taken the lowest pressure in the system which is at the outlet to be zero with the understanding that this is a relative value. Undoubtedly, as is the case for the hydraulic conductivity mentioned earlier, the flow rate values vary considerably over the day and also are not the same for every individual. Variation in the eye size is also an important factor. Therefore, the values given here are by no means precise.

The interface conditions are as follows:

$$P_{\mathrm{L}} = P_{\mathrm{G}} \tag{5}$$

$$\boldsymbol{u}_{\mathrm{L}}\cdot\boldsymbol{n} = \boldsymbol{u}_{\mathrm{G}}\cdot\boldsymbol{n}, \quad -\frac{K_{\mathrm{L}}}{\mu}(\nabla P_{\mathrm{L}}\cdot\boldsymbol{n}) = -\frac{K_{\mathrm{G}}}{\mu}(\nabla P_{\mathrm{G}}\cdot\boldsymbol{n}) \tag{6}$$

The iterative approach for deriving pressure distribution throughout vitreous is carried out as follows:

An initial-guess pressure value is assigned to all interfacial nodes ($P_{\mathrm{int}} = P_0$). By assigning an initial pressure value (P_0) at the interfacial nodes, the boundary conditions for the nonliquefied zone become sufficient. A nonhomogeneous Dirichlet boundary condition (initial guess on interface) and a combination of Neumann/Dirichlet boundary conditions (outlet, inlet, outer surface) are applied. Hence, the pressure values of the porous zone are obtained. Velocity distribution at the interfacial elements is obtained using the pressure distribution. Based on the interface condition (6), the boundary condition for liquefied zone is determined (nonhomogeneous Neumann boundary condition on interface). Pressure distribution in the liquefied region is obtained and the initial pressure (P_0) on interface is replaced with new pressure values. This iterative process continues until the difference between the new pressure values and the previous ones becomes sufficiently low. At that point, the process is considered to have converged and the code stops, giving the pressure distribution throughout the whole vitreous.

Pressure distribution in the nonliquefied (gel) zone:

Governing equation

$$\nabla^2 P_{\mathrm{G}} = 0 \tag{7}$$

Boundary condition (outer surface except inlet and outlet)

$$\nabla P_{\mathrm{G}}\cdot\boldsymbol{n} = 0 \tag{8}$$

Boundary condition (inlet)

$$\nabla P_{\mathrm{G}} = -\frac{\mu}{K_{\mathrm{G}}}\boldsymbol{u}_{\mathrm{in}} \tag{9}$$

Boundary condition (outlet)

$$P_{\mathrm{G}} = P_{\mathrm{out}} = 0 \tag{10}$$

Gel–liquid interface condition

$$P_{\mathrm{G}} = P_0 \tag{11}$$

where P_0 is the initial guess for the pressure values at the interfacial nodes. With the gel region pressure distribution completely determined based on this initial guess, the normal velocity at the interface is calculated and applied to the liquid region. With the liquid region completely solved, the pressure at the interface is obtained as an updated value, which is then applied in place of P_0

in Eq. (11). This process is repeated iteratively until consistent interface pressure distribution is obtained. The velocity $\boldsymbol{u}_{\text{in}}$ is known as mentioned earlier (see Eq. (4)).

Governing equation in the liquefied zone

$$\nabla^2 P_{\text{L}} = 0 \tag{12}$$

Boundary condition (interface)

$$\nabla P_{\text{L}} \cdot \boldsymbol{n} = -\frac{\mu}{K_{\text{L}}} \boldsymbol{u}_{\text{int}} \cdot \boldsymbol{n} \tag{13}$$

The results provide velocity and pressure distribution in both regions. One example depicting flow streamlines and isobars is shown above in Fig. 3. Additional results for various geometries are given in Sec. 4 under Results and Discussion.

3.2 Drug Concentration Distribution. To solve the convection–diffusion equation Galerkin FEM has been in common use. However, as is well-known, Galerkin method does not capture the right behavior of a convective–diffusive model when the Péclet number is higher than one and the results can be unstable. According to Padilla Montero [32], when the Péclet number of a mesh is higher than 1, the Galerkin method is unsuitable. To stabilize the model, Petrov–Galerkin method was successfully applied. In this method, a new residual formulation is employed. This formulation includes the original weak formulation with some extra stabilization terms.

The Crank–Nicolson scheme was applied to discretize the partial derivative with respect to time in the transient convection-diffusion equation, i.e.,

$$\frac{\partial C}{\partial t} = D\nabla^2 C - \boldsymbol{u} \cdot \nabla C$$

$$\text{Crank-Nicolson:} \quad \frac{\Delta C}{\Delta t} = \frac{1}{2}\left(\frac{\partial C^n}{\partial t} + \frac{\partial C^{n+1}}{\partial t}\right)$$

For a porous medium, we normally adjust the advection term with a liquid volume fraction. However, in the case of the vitreous, the fraction is close to unity. After a few simplifications, this equation can be expressed as

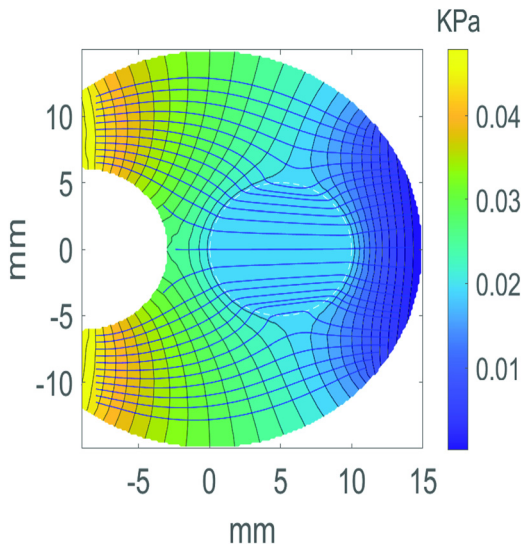

Fig. 3 Flow field in the heterogeneous vitreous. The spherical liquefied region is shown by a white dashed circle. Flow streamlines go from left to right, with some passing nearly horizontally through the liquefied region. Isobars are orthogonal to the streamlines. The origin is indicated by a black dot.

$$\frac{\Delta C}{\Delta t} + \frac{1}{2}\boldsymbol{u} \cdot \nabla(\Delta C^n) - \frac{1}{2} D\nabla^2(\Delta C^n) = -\boldsymbol{u} \cdot \nabla(C^n) + D\nabla^2(C^n) \tag{14}$$

The boundary condition around the vitreous is

$$\nabla C \cdot \boldsymbol{n} = 0 \tag{15}$$

except for the inlet and the outlet where

$$(\boldsymbol{u}C - D\nabla C) \cdot \boldsymbol{n} = h_p C \tag{16}$$

Here, $\boldsymbol{n}$ is the outward unit normal vector and h_p corresponds to the respective permeability values (hyaloid and RPE), which may be nondimensionalized as the Biot number, $\text{Bi} = h_p l/D$. Here, Bi number is chosen to be 0.01. The parameter l is the length scale for our model, which is assumed to be equal to the diameter of the eye (30 mm). The Biot number value is by no means precise and depends on the permeability of the specific drug and the availability of measurements which, especially for macromolecular drugs, are sparse. Convective transport through the boundary is permitted as it carries the macromolecular drugs through the boundary to the blood vessels. The initial condition for the system consists of a 30 μl intravitreal injection of a drug bolus of initial concentration C_0. This is distributed by diffusion and convection and eventually reaches the retina. Since the system equations are linear, the distribution will be proportional to the C_0 and we therefore scale the concentration with this value. Thus, the scaled initial concentration of the bolus is unity.

For the computations, we have used the parameter τ, which is the intrinsic time or stabilization parameter. In this model, τ was defined as

$$\tau = \left[\left(\frac{2|\boldsymbol{u}|}{h}\right) + \left(\frac{4D}{h^2}\right)\right]^{-1}, \tag{17}$$

where

$$|\boldsymbol{u}|\text{: Average velocity in a mesh} \tag{18}$$

$$h\text{: Mesh size} \tag{19}$$

$$D\text{: Diffusion coefficient} \tag{20}$$

In order to achieve stability, h was defined as the maximum length of the lines connecting each corner to the center of its opposite triangular face. More details of the computational development are given in the Supplemental Material on the ASME Digital Collection.

4 Results and Discussion

The mesh that was chosen for this simulation consisted of 15,549 nodes and 83,303 unstructured tetrahedral elements. The inlet velocity from the aqueous humor to the vitreous via the hyaloid membrane based on volumetric flow rates of 3 μl/min was calculated to be $\boldsymbol{u}_{\text{in}} = [0.000147 \quad 0 \quad 0]$ mm/s. Two values were chosen for the diffusion coefficient D, to represent moderate

Table 1 Flow rate per pressure drop variation with the amount of liquefaction (see the plots in Fig. 5)

Liquefied region	Volume fraction (%)	Flow rate/pressure drop (mm^3/(Pa · s))
$R = 2$ mm	0.66	59.3
$R = 3$ mm	2.23	61.1
$R = 5$ mm	10.33	67.6
$R = 7$ mm	28.35	83.0

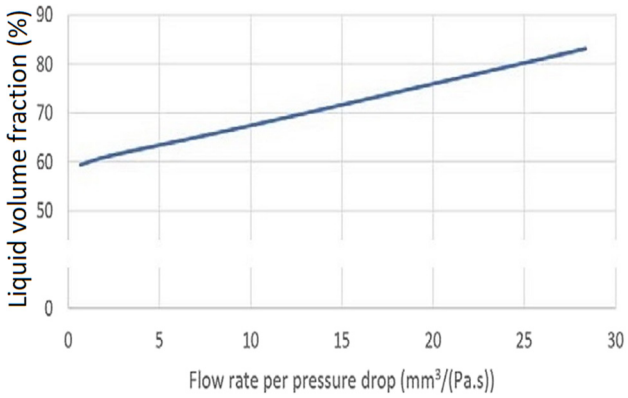

Fig. 4 Flow rate per pressure drop versus the volume fraction of the liquefied region

and high Péclet numbers. The higher diffusion coefficient D is taken to be 10^{-5} mm^2/s [17] and the lower one as 1.67×10^{-8} mm^2/s, which corresponds to macromolecules. There have been several recent studies on the measurement of the diffusion coefficient of large molecules in the vitreous humor (see Penkova et al. [33], Rattanakijsuntorn et al. [34], Zhang et al. [35]). Also, a catalog of diffusion coefficient values has been provided in the review by Penkova [36]. For the inlet velocity of 0.000147 mm/s, the two chosen diffusion coefficients values represent Péclet numbers 2.652×10^5 and 4.42×10^2.

Simulation results are divided into two sections: Fluid Mechanics and Mass Transfer.

4.1 Fluid Mechanics. The following simulation results include different locations and sizes for the liquefied region and different initial conditions for bolus.

The values in the Eq. (4) correspond to physiological condition driving the flow. For a living eye, flow rate is not a controllable parameter. Therefore, we rely on measured volumetric flow based on previous studies [31] to calculate the inlet velocities as mentioned earlier. The total outflow would be based on the same volumetric flow rate. But this is not specified since the pressure at the outlet is assigned a value.

The interesting feature of the fluid flow results in the convergence of the streamlines into the liquid region as shown in Fig. 3. This is to be expected since with pressure as the driving potential, the flow chooses the path of least resistance and converges into

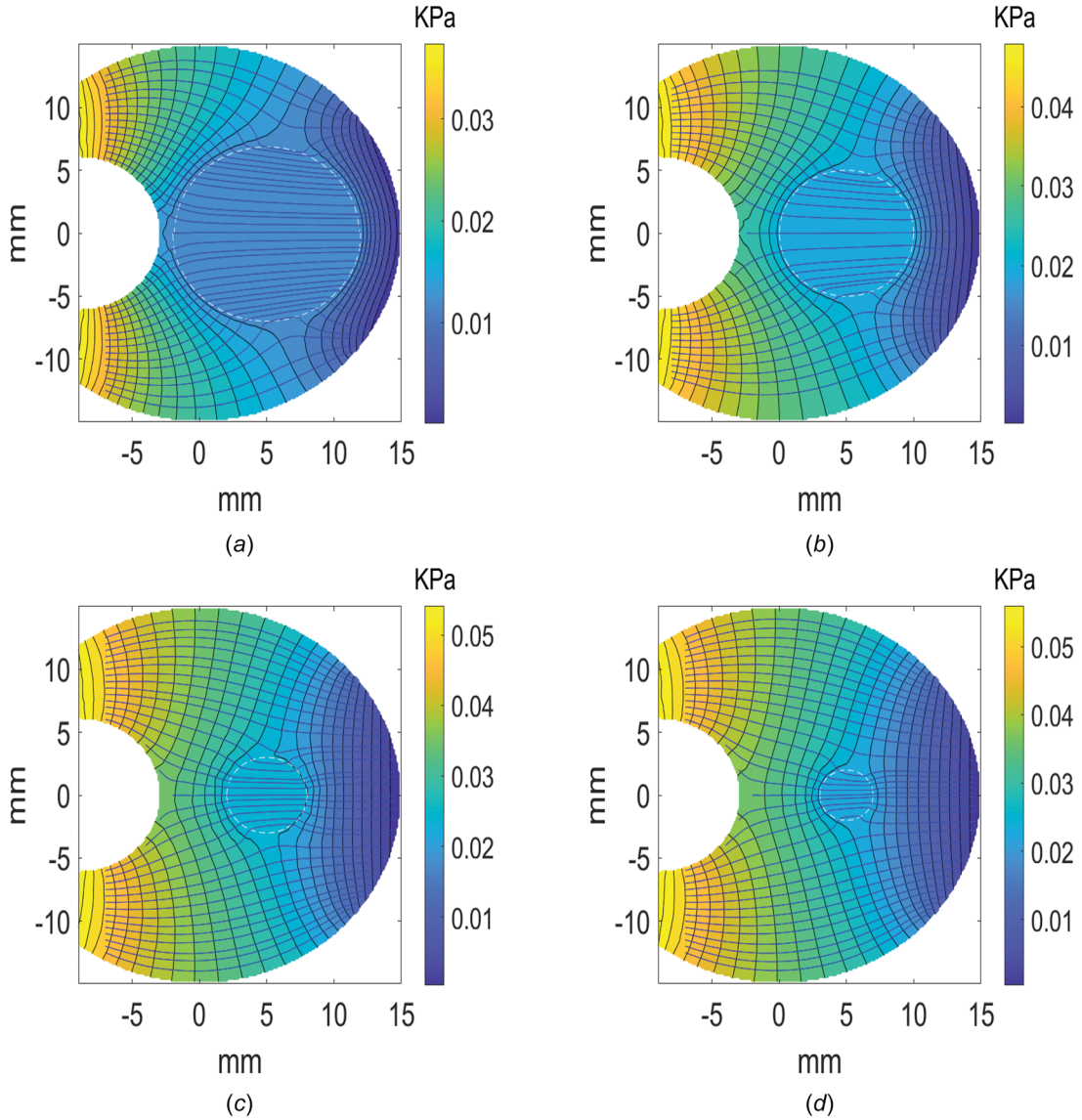

Fig. 5 Streamlines and isobars. The liquefied region is a sphere with the center position located at (5, 0, 0)mm for various radii: (*a*) *R*: 7 mm, (*b*) *R*: 5 mm, (*c*) *R*: 3 mm, and (*d*) *R*: 2 mm.

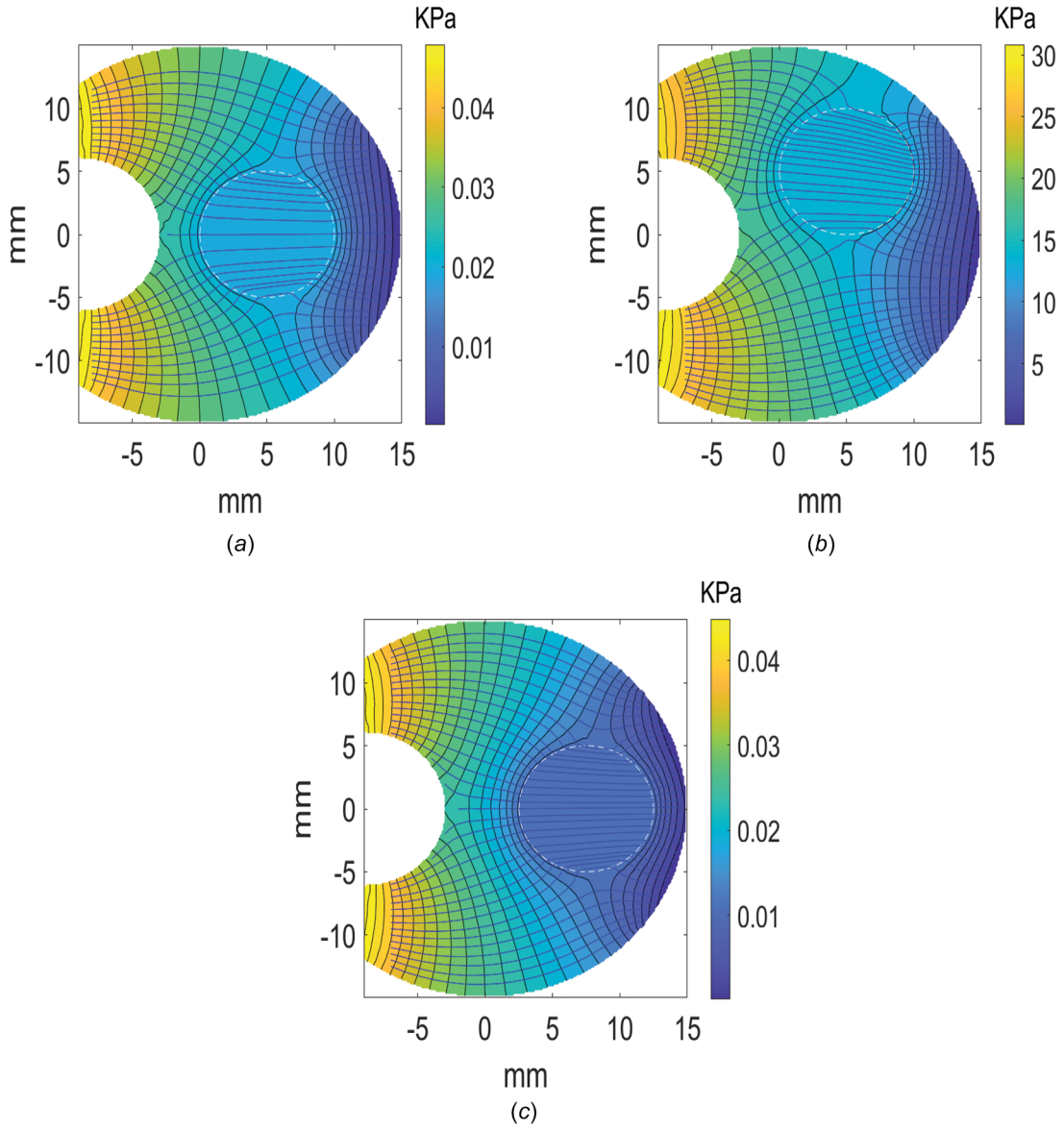

Fig. 6 Streamlines and isobars, the liquefied region is a sphere and the center position is given by *C* with radius of 5 mm: (*a*) *C*: (5, 0, 0) mm, (*b*) *C*: (5, 5, 0) mm, and (*c*) *C*: (7.5, 0, 0) mm

the liquid region that has effectively very high permeability. For a given average pressure drop across the vitreous, the flow rate increases with increasing the level of liquefaction. Again, this is not unexpected since the free mobility in the liquid region affords much lower resistance to the flow. We have tabulated the flow rate per pressure drop values as a function of the liquid volume fraction (Table 1).

These results have been plotted in Fig. 4, indicating a remarkably linear relationship between the flow rate per pressure drop and the volume fraction. The corresponding flow streamlines and isobars are given in Fig. 5. Flow rate per pressure drop values for various cases in Fig. 6 was calculated and is found to remain almost constant, which is expected as the volume fraction of the liquefied region does not change. In all the figures, the flow field illustrations are in the *xy*-plane.

We have considered another interesting case in which the liquefied region is in contact with retina. The boundary conditions as given by Eqs. (4), and (10) where the exit pressure condition applies to both the liquid and the gel regions in contact with the retina. Here, we find significant distortion of flow streamlines with convergence into the liquefied region (as shown in Fig. 7).

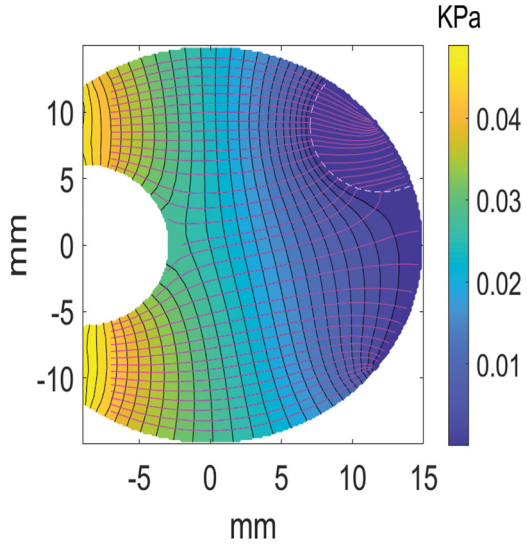

Fig. 7 Pressure distribution and flow streamlines, liquefied region is in contact with retina with boundary condition (4)

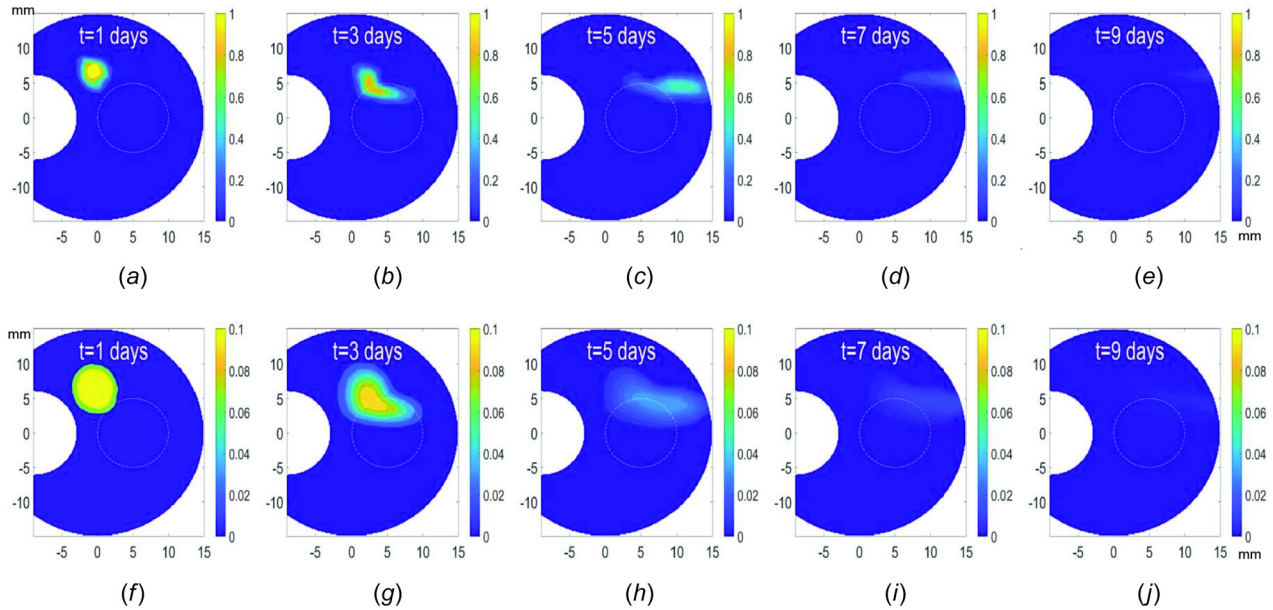

Fig. 8 Macromolecular drug transport in the vitreous. The concentration intensity bar represents the dimensionless concentration scaled with the initial bolus concentration. The spherical liquefied region (5 mm radius) located on the eye centerline, positioned at (5, 0, 0)mm. The bolus is initially injected at (−2, 7, 0)mm. (*a*)–(*e*) display the results for Pe = 2.652×10^5 while (*f*)–(*j*) are for Pe = 4.42×10^2.

4.2 Mass Transfer. As already mentioned, for the mass transfer calculations, the initial bolus injection is taken to be a concentration of unity, which represents the nondimensional value scaled with respect to an initial distribution. Various cases of eye topography have been considered, and the results are displayed in Figs. 8–15. For the moderate Péclet number cases, the concentration intensity bar is cut off at a dimensionless concentration value of 0.1 or lower in order to maintain the visibility of low concentration values at longer times. Figure 8 depicts the transport of macromolecules throughout the vitreous over time. The white dashed line circles the liquefied zone. It can be concluded from the figures that the movement of macromolecules in this zone is much faster than their movement in the porous medium. The drug transport history for Péclet numbers 2.652×10^5 and 4.42×10^2.

The importance of developing a mathematical model for the transport of macromolecules in a partially liquefied vitreous is displayed in Figs. 8–15. For high and moderate Péclet numbers, we have analyzed various scenarios concerning the liquefied region to ascertain the impact of its topography on drug transport. The different situations include changing the liquid region position and size and also the relative position of the initial injection site. In Fig. 8, drug was initially injected at $(-2, 7, 0)$, whereas in Fig. 9, it is injected 4 mm higher at $(-2, 11, 0)$. The results for the drug pathways, as we can observe, have quite different characterizations, depending on the injection location. The former is a bit closer to the liquefied region; therefore, it is completely drawn into it while the latter does not enter the liquefied region and moves through the nonliquefied region the whole time. In conclusion, in a partially liquefied vitreous, the initial injection point of the drug becomes considerably more important as the passageway of the macromolecules could completely differ as the location of the injection point relative to the liquefied region slightly changes.

From the results presented in Figs. 8, 10, and 11, we can observe the effect of changes in the location of the liquefied

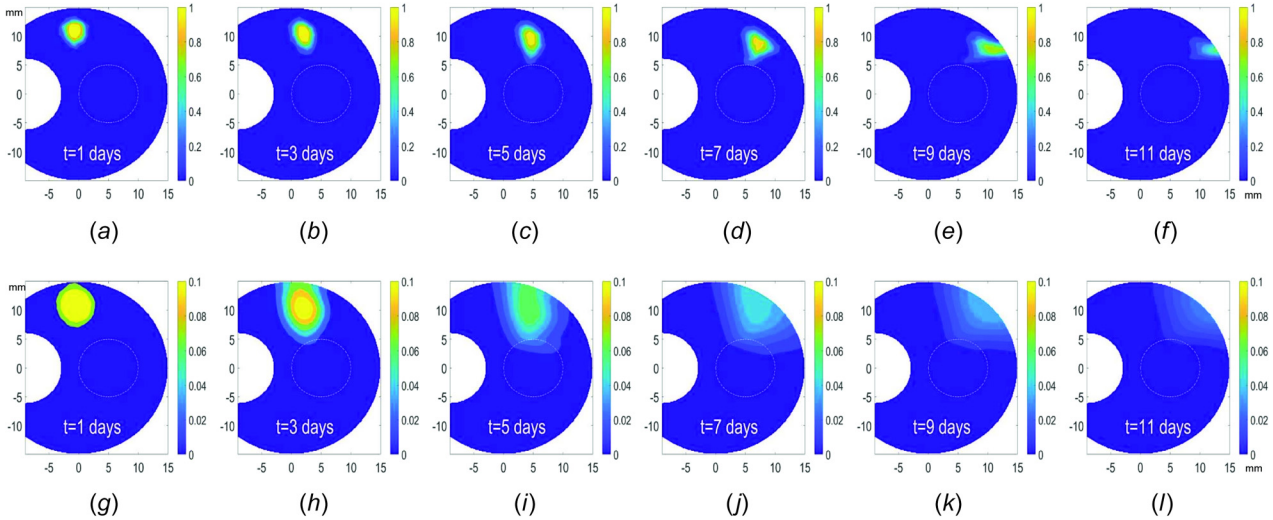

Fig. 9 Same geometry as Fig. 8. The drug bolus injection location is shifted higher to the point (−2, 11, 0)mm. (*a*)–(*f*) display the results for Pe = 2.652×10^5 and (*g*)–(*l*) represent Pe = 4.42×10^2.

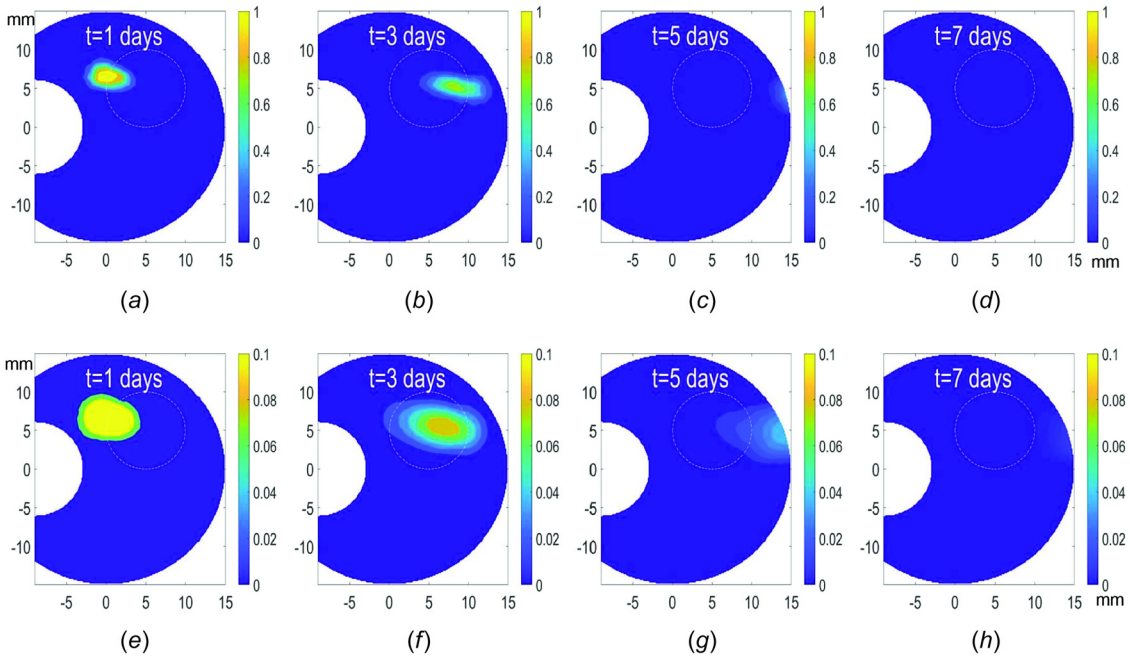

Fig. 10 Drug transport in the vitreous with asymmetrically positioned liquid region, centered at (5, 5, 0)mm and 5 mm radius with bolus initially injected at (−2, 7, 0)mm. (*a*)–(*d*) display the results for Pe = 2.652×10^5 and (*e*)–(*h*) correspond to Pe = 4.42×10^2.

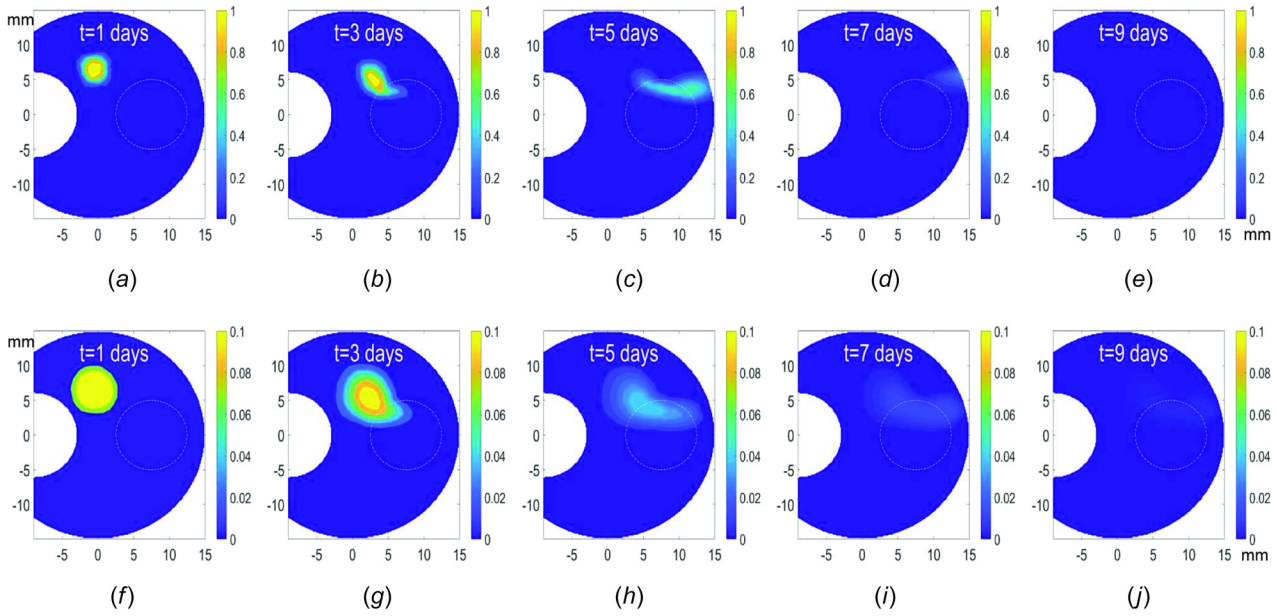

Fig. 11 Similar geometry and initial injection location as Fig. 8, except that the liquid spherical region is placed further back centered at (7.5, 0, 0)mm. (*a*)–(*e*): Pe = 2.652×10^5 and (*f*)–(*j*): Pe = 4.42×10^2.

region on macromolecular drugs transport. As the liquefied region gets closer to either the initial drug injection point or the outlet (retina), macromolecules require less time to reach the retina. This is of course due to the drug being channeled through the liquid region where the flow constriction gives it a higher velocity. With the drug being transported through this region, faster transport rate is inevitable.

In Figs. 8, 12, and 13, the center of the liquefied region is located at the same point but the radius varies. Not surprisingly, by increasing size of the liquefied region, the drug arrives at retina much faster.

The contact location of the macromolecular drug with retina is of considerable importance when treating different ocular diseases. In Fig. 14, a case is presented in which the presence of the liquefied region has slightly changed the contact location of the drug with retina (pressure distribution of this case is presented in Fig. 7 in the Fluid Mechanics section). The drug movement starting from the centerline just behind the lens travels to retina several millimeters higher as seen in Fig. 14.

5 Conclusion

In this paper, we have successfully simulated drug distribution in a partially liquefied vitreous over time in three dimensions. Such work representing drug transport in a syneretic eye does not appear to have been done in previous studies.

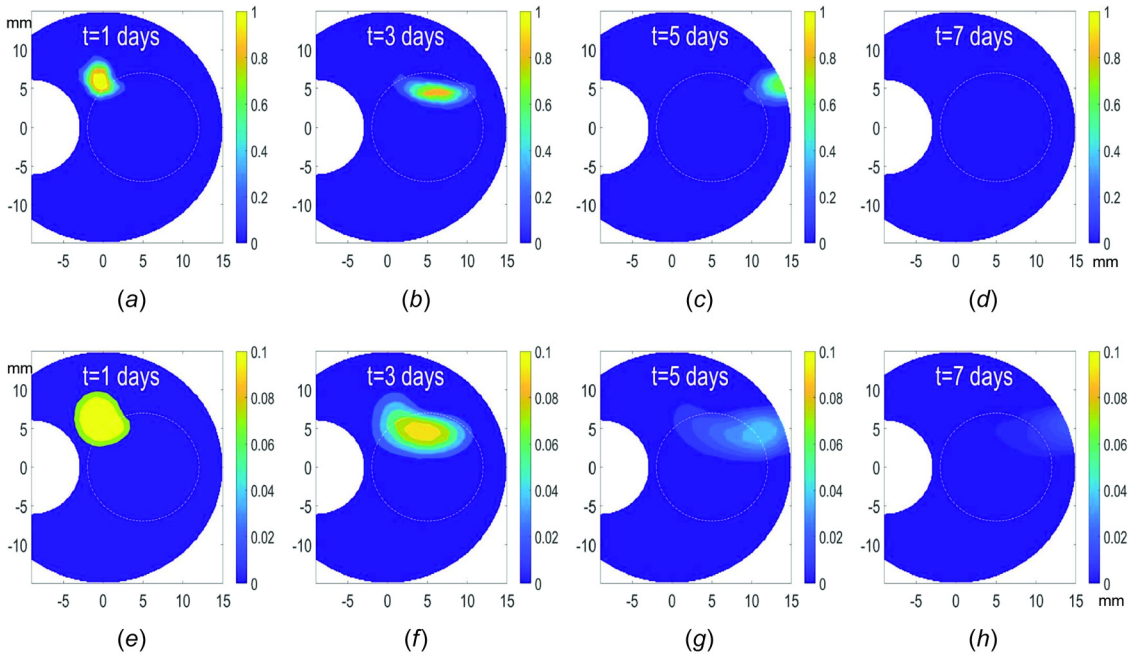

Fig. 12 Drug transport through the liquefied region. The initial injection position is the same as Fig. 11. This case is also axisymmetric but liquid sphere with 7 mm radius is larger than the case in Fig. 8 (5 mm). (*a*)–(*d*) display the results for Pe = 2.652×10^5 and (*e*)–(*h*) correspond to Pe = 4.42×10^2.

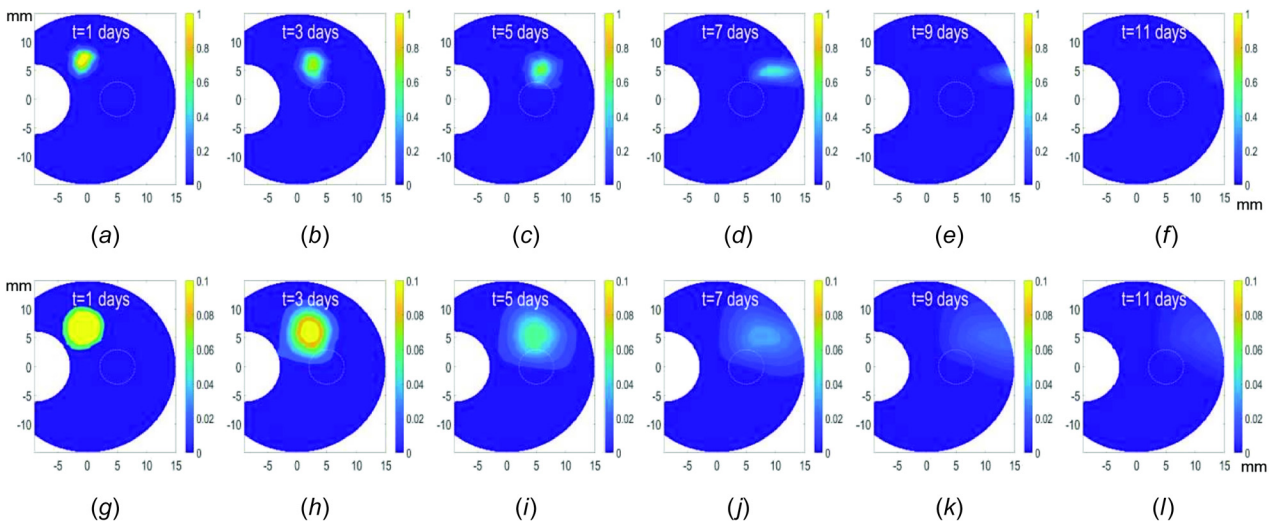

Fig. 13 Same characteristics as Fig. 12 but with a smaller liquid region (3 mm radius). (*a*)–(*f*) correspond to the results for Pe = 2.652×10^5 and (*g*)–(*l*) represent Pe = 4.42×10^2.

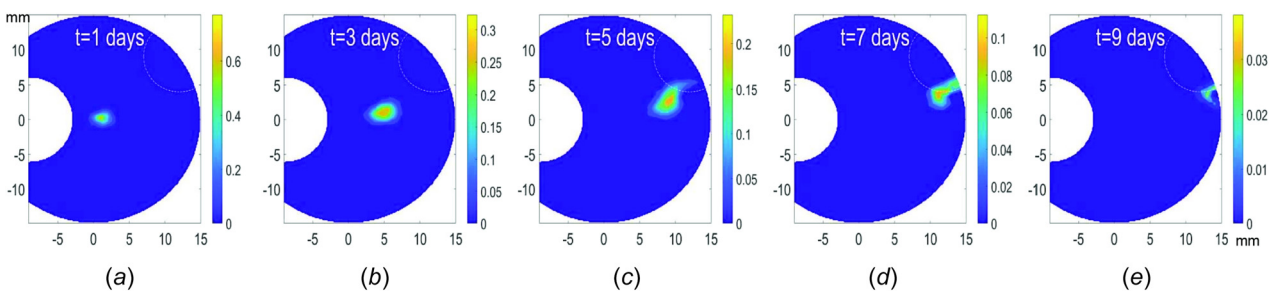

Fig. 14 Liquefied region is in contact with retina with boundary condition (4) for high Péclet flow

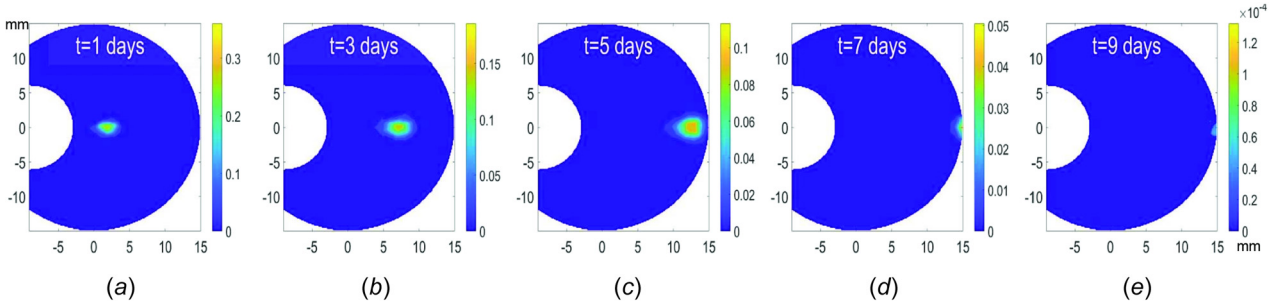

Fig. 15 Case having no liquefied region with boundary condition (4) for high Péclet number flow

Our mathematical model provides fluid flow and drug transport characteristics within a partially liquefied vitreous. Among the fundamentally interesting features emanating from this investigation include the fluid-flow characteristics in a heterogeneous vitreous. In particular, we see the convergence of the streamlines into the liquefied region as the flow chooses paths of least resistance. As for drug delivery, the convection-dominated transport follows these streamlines accompanied by diffusion. The model will provide useful prediction of the drug pathways and delivery location based on the specific eye topographies. The topography with the vitreous varies for different individuals and may present advantages or disadvantages in terms of targeting drugs. In either case, the predictive modeling will be helpful in providing scientifically sound information on suitable locations for injection.

Our future effort will include broadening the scope of the model to accommodate various shapes of the liquefied region and impact on the overall delivery starting from a specific vitreous location. In addition, a great deal of improvement of the fluid-flow modeling needs to be carried out. Specifically, as mentioned in Sec. 2, effects such as saccadic motion and vitreous structural flexibility need to be investigated. Furthermore, the modeling of drug-clearance characterization with choroidal blood flow needs to be included for a more comprehensive model. It also needs to be mentioned that the current input parameters such as flow rate are subject to considerable variation, and a sensitivity analysis is appropriate. These are significant tasks that require a considerable effort, and are a part of ongoing and future investigations.

Funding Data

- National Eye Institute under the NIH (Grant No. 5R01EY026599; Funder ID: 10.13039/100000002).

Conflict of Interest

The authors report no conflict of interest.

Nomenclature

Bi = $h_p l/D$, mass-transfer Biot number
C = liquefied region center position
C = drug concentration
C = drug concentration
C_0 = initial drug concentration
D = diffusion coefficient
h = mesh size
h_p = RPE permeability
K = Darcy coefficient
l = length scale: eye diameter
n = unit normal
P = pressure
Pe = Péclet number
R = liquefied region radius
RPE = retinal pigment epithelium
t = time
u = velocity
x_i = coordinates

Greek/Math Symbols

μ = liquid viscosity
τ = intrinsic time; stabilization parameter
$\mathbf{\Phi}$ = vector with ϕ_i elements (Supplemental Material on the ASME Digital Collection)
∇ = gradient operator

Subscripts/Superscripts

G = gel part of the vitreous
L = liquid part of the vitreous
i = L or G; node symbolism (1, 2, 3, 4)
In = inlet
int = interface
nint = not on interface
L = liquid part of the vitreous
mesh = pertaining to the mesh
out = outlet
T = transpose
0 = initial guess

References

[1] Lamminsalo, M., Taskinen, E., Karvinen, T., Subrizi, A., Murtomäki, L., Urtti, A., and Ranta, V. P., 2018, "Extended Pharmacokinetic Model of the Rabbit Eye for Intravitreal and Intracameral Injections of Macromolecules: Quantitative Analysis of Anterior and Posterior Elimination Pathways," Pharm. Res., **35**(8), pp. 1531–1514.

[2] Kuno, N., and Fuji, S., 2010, "Biodegradable Intraocular Therapies for Retinal Disorders: Progress to Date," Drugs Aging, **27**(2), pp. 117–134.

[3] Iovino, C., Mastropasqua, R., Lupidi, M., Bacherini, D., Pellegrini, M., Bernabei, F., Borrelli, E., Sacconi, R., Carnevali, A., D'Aloisio, R., Cerquaglia, A., Finocchio, L., Govetto, A., Erba, S., Triolo, G., Di Zazzo, A., Forlini, M., Vagge, A., and Giannaccare, G., 2020, "Intravitreal Dexamethasone Implant as a Sustained Release Drug Delivery Device for the Treatment of Ocular Diseases: A Comprehensive Review of the Literature," Pharmaceutics, **12**(8), p. 703.

[4] Lee, S. S., and Robinson, M. R., 2009, "Novel Drug Delivery Systems for Retinal Diseases," Ophthal. Res., **41**(3), pp. 124–135.

[5] Haghjou, N., Abdekhodaie, M., Cheng, Y. L., and Saadatmand, M., 2011, "Computer Modeling of Drug Distribution After Intravitreal Administration," W. A. S. Eng. Technol., **52**(5), pp. 194–204. ISNI:0000000091950263

[6] Kathawate, J., and Acharya, S., 2008, "Computational Modeling of Intravitreal Drug Delivery in the Vitreous Chamber With Different Vitreous Substitutes," Int. J. Heat Mass Transfer, **51**(23–24), pp. 5598–5609.

[7] Tojo, K., and Isowaki, A., 2001, "Pharmacokinetic Model for In Vivo/In Vitro Correlation of Intravitreal Drug Delivery," Adv. Drug Deliv. Rev., **52**(1), pp. 17–24.

[8] Missel, P., 2012, "Simulating Intravitreal Injections in Anatomically Accurate Models for Rabbit, Monkey, and Human Eyes," Pharmaceut. Res., **29**(12), pp. 3251–3272.

[9] Zhang, Y., Bazzazi, H., Lima e Silva, R., Pandey, N. B., Green, J. J., Campochiaro, P. A., and Popel, A. S., 2018, "Three-Dimensional Transport Model for Intravitreal and Suprachoroidal Drug Injection," Invest. Ophtalmol. Vis. Sci., **59**(12), pp. 5266–5276.

[10] Avtar, R., and Tandon, D., 2008, "A Mathematical Analysis of Intravitreal Drug Transport," Tropical J. Pharm. Res., **7**(1), pp. 867–877.

[11] Balachandran, R., and Barocas, V., 2008, "Computer Modeling of Drug Delivery to the Posterior Eye: Effect of Active Transport and Loss to Choroidal Blood Flow," Pharm. Res., **25**(11), pp. 2685–2696.
[12] Araie, M., and Maurice, D., 1991, "The Loss of Fluorescein, Fluorescein Glucuronide and Fluorescein Isothiocyanate Dextran From the Vitreous by the Anterior and Retinal Pathways," Exp. Eye Res., **52**(1), pp. 27–39.
[13] Ohtori, A., and Tojo, K., 1994, "In Vivo/In Vitro Correlation for Intravitreal Delivery of Drugs With the Help of Computer Simulation," Biol. Pharm. Bull., **17**(2), pp. 283–290.
[14] Friedrich, S., Cheng, Y. L., and Saville, B., 1997, "Finite Element Modeling of Drug Distribution in the Vitreous Humor of the Rabbit Eye," Ann. Biomed. Eng., **25**(2), pp. 303–314.
[15] Lin, H., 2004, "Finite Element Modeling of Drug Transport Processes After an Intravitreal Injection," Master's thesis, University of Toronto, Toronto, ON, Canada.
[16] Xu, J., Heys, J., Barocas, V. H., and Randolph, T. W., 2000, "Permeability and Diffusion in Vitreous Humor: Implications for Drug Delivery," Pharm. Res., **17**(6), pp. 664–669.
[17] Stay, M. S., Xu, J., Randolph, T. W., and Barocas, V. H., 2003, "Computer Simulation of Convective and Diffusive Transport of Controlled-Release Drugs in the Vitreous Humor," Pharm. Res., **20**(1), pp. 96–102.
[18] Park, J., Bungay, P. M., Lutz, R. J., Augsburger, J. J., Millard, R. W., Sinha Roy, A., and Banerjee, R. K., 2005, "Evaluation of Coupled Convective-Diffusive Transport of Drugs Administered by Intravitreal Injection and Controlled Release Implant," J. Control Release, **105**(3), pp. 279–295.
[19] Meskauskas, J., Repetto, R., and Siggers, J. H., 2011, "Oscillatory Motion of a Viscoelastic Fluid Within a Spherical Cavity," J. Fluid Mech., **685**, pp. 1–22.
[20] Bayat, J., Emdad, H., and Abouali, O., 2020, "Numerical Investigation of Partially Liquefied Vitreous Dynamics as Two-Phase Viscoelastic-Newtonian Fluid Flow in a Planar Cavity Due to Oscillatory Motion," Int. J. Multiphase Flow, **127**, p. 103259.
[21] Huang, J., and Gharib, M., 2021, "Thermal Effects on Fluid Mixing in the Eye," Ann. Biomed. Eng., **49**(1), pp. 251–261.
[22] Narasimhan, A., and Sundarraj, C., 2015, "Convection-Enhanced Intravitreous Drug Delivery in Human Eye," ASME J. Heat Transfer-Trans. ASME, **137**(2), p. 121003.
[23] Mukundakrishnan, K., and Ayyaswamy, P. S., 2011, "Transport and Diffusion Analyses as Applied in Biomaterials Studies" *Comprehensive Biomaterials*, P. Ducheyne, K. Healy, D. Hutmacher, D. Grainger, and C. Kirkpatrick, eds., Vol. 3, Elsevier, Amsterdam, The Netherlands, pp. 133–153.
[24] Kim, H., Lizak, M. J., Tansey, G., Csaky, K. G., Robinson, M. R., Yuan, P., Wang, N. S., and Lutz, R. J., 2005, "Study of Ocular Transport of Drugs Released From an Intravitreal Implant Using Magnetic Resonance Imaging," Ann. Biomed. Eng., **33**(2), pp. 150–164.
[25] Penkova, A., Zhang, S., Humayun, M., Fraser, S., Moats, R., and Sadhal, S. S., 2020, "Measurement of the Hydraulic Conductivity of the Vitreous Humor," J. Porous Media, **23**(2), pp. 195–206.
[26] Scott, J. E., 1992, "The Chemical Morphology of the Vitreous," Eye, **6**(6), pp. 553–555.
[27] Ai, L., and Vafai, K., 2006, "A Coupling Model for Macromolecule Transport in a Stenosed Arterial Wall," Int. J. Heat Mass Transfer, **49**(9–10), pp. 1568–1591.
[28] Khanafer, K., and Vafai, K., 2006, "The Role of Porous Media in Biomedical Engineering as Related to Magnetic Resonance Imaging and Drug Delivery," Heat Mass Transfer, **42**(10), pp. 939–953.
[29] Vafai, K., 2011, *The Role of Porous Media in Biomedical Engineering as Related to Magnetic Resonance Imaging and Drug Delivery*, CRC Press, Boca Raton, FL.
[30] Vafai, K., 1984, "Convective Flow and Heat Transfer in Variable-Porosity Media," J. Fluid Mech., **147**(1), pp. 233–259.
[31] Pang, I., and Clark, A. F., 2008, "Chapter 3: IOP as a Target—Inflow and Outflow Pathways," *Ocular Therapeutics*, T. Yorio, A. F. Clark, and M. B. Wax, eds., Academic Press, London, pp. 45–67.
[32] Montero, I. P., 2014, "Numerical Implementation of a Mixed Finite Element Formulation for Convection-Diffusion Problems," Bachelor's thesis, Polytechnic University of Catalonia, Barcelona, Catalonia, Spain.
[33] Penkova, A., Rattanakijsuntorn, K., Sadhal, S., Tang, Y., Moats, R., Hughes, P. M., Robinson, M. R., and Lee, S. S., 2014, "A Technique for Drug Surrogate Diffusion Coefficient Measurement by Intravitreal Injection," Int. J. Heat Mass Transfer, **70**, pp. 504–514.
[34] Rattanakijsuntorn, K., Penkova, A., and Sadha, S. S., 2018, "Mass Diffusion Coefficient Measurement for Vitreous Humor Using FEM and MRI," IOP Conf. Ser. Mater. Sci. Eng., **297**, p. 012024.
[35] Zhang, S., Penkova, A., Humayun, M. S., Martinez-Camarillo, J. C., Tadle, A. C., Galesic, A., Thompson, M. E., Pratt, M., Gonzales-Calle, A., and Sadhal, S. S., 2021, "In Vivo Experimental and Analytical Studies for Bevacizumab Diffusion Coefficient Measurement in the Rabbit Vitreous Humor," ASME J. Heat Transfer-Trans. ASME, **143**(3), p. 032101.
[36] Penkova, A., Moats, R., Humayun, M., Fraser, S., and Sadhal, S. S., 2019, "Diffusive Transport in the Vitreous Humor: Experimental and Analytical Studies," ASME J. Heat Transfer-Trans. ASME, **141**(5), p. 050801.